Supplementary Information for

Emergent zero-field anomalous Hall effect in a reconstructed rutile antiferromagnetic metal

Meng Wang[1,*,†], Katsuhiro Tanaka[2,†], Shiro Sakai[1], Ziqian Wang[1], Ke Deng[3,4], Yingjie Lyu[5], Cong Li[5], Di Tian[5], Shengchun Shen[6], Naoki Ogawa[1,7], Naoya Kanazawa[8], Pu Yu[5], Ryotaro Arita[1,2], Fumitaka Kagawa[1,9,*]

[1]*RIKEN Center for Emergent Matter Science (CEMS), Wako, 351-0198, Japan.*

[2]*Research Center for Advanced Science and Technology, University of Tokyo, Tokyo 153-8904, Japan.*

[3]*Shenzhen Institute for Quantum Science and Engineering, Southern University of Science and Technology (SUSTech), Shenzhen 518055, China.*

[4]*International Quantum Academy, Shenzhen 518048, China.*

[5]*State Key Laboratory of Low Dimensional Quantum Physics and Department of Physics, Tsinghua University, Beijing, 100084, China.*

[6]*Department of Physics, University of Science and Technology of China, Hefei, 230026, China.*

[7]*Department of Applied Physics and Quantum-Phase Electronics Center (QPEC), University of Tokyo, Tokyo 113-8656, Japan.*

[8]*Institute of Industrial Science, The University of Tokyo, Tokyo 153-8505, Japan.*

[9]*Department of Physics, Tokyo Institute of Technology, Tokyo 152-8551, Japan.*

[*]Corresponding authors. Email: meng.wang@riken.jp; fumitaka.kagawa@riken.jp

[†]These authors contributed equally: Meng Wang, Katsuhiro Tanaka.

Supplementary Fig. 5, **Transport properties in $Ru_{1-x}Cr_xO_2$ (110) and the x = 0.2 film with current along different directions.**

Supplementary Fig. 6, **Magnetization measurements in a $Ru_{0.8}Cr_{0.2}O_2$ (110) film.**

Supplementary Fig. 7, **Magnetic-field dependent Hall conductivity at various temperatures**.

Supplementary Fig. 8, **Scaling of $\sigma_{xy}^{M} \sim \sigma_{xx}$ in the $Ru_{0.8}Cr_{0.2}O_2$ (110) films**.

Supplementary Fig. 9, **Magnetoresistivity (MR) measured for the $Ru_{0.8}Cr_{0.2}O_2$ (110) film**.

Supplementary Note 1, Symmetry analysis of AHE for rutile RuO_2:

The Hall vector $\boldsymbol{\sigma}_{Hall} = (\sigma_{yz}, \sigma_{zx}, \sigma_{xy})$, is defined as in reference 14. The RuO_2 with the Néel vector along the [001] direction has a magnetic space group (MSG) of $P4_2'/mnm'$. The $P4_2'/mnm'$ has $\boldsymbol{t}_{1/2}\boldsymbol{C}_{2x}$ and $\boldsymbol{t}_{1/2}\boldsymbol{C}_{2y}$ symmetry operations, where $\boldsymbol{C}_{2x}$ ($\boldsymbol{C}_{2y}$) is an operation of rotating 180° along the x (y) axis and $\boldsymbol{t}_{1/2}$ denotes a translation (a/2, b/2, c/2), which correspond to $\boldsymbol{C}_{2x}$ and $\boldsymbol{C}_{2y}$ in the magnetic point group (MPG). Furthermore, $\boldsymbol{C}_{2x}(\sigma_{yz}, \sigma_{zx}, \sigma_{xy}) = (\sigma_{yz}, -\sigma_{zx}, -\sigma_{xy})$ and $\boldsymbol{C}_{2y}(\sigma_{yz}, \sigma_{zx}, \sigma_{xy}) = (-\sigma_{yz}, \sigma_{zx}, -\sigma_{xy})$, demonstrate $\boldsymbol{\sigma}_{Hall} = \mathbf{0}$; i.e., σ_{yz}, σ_{zx},and σ_{xy} are all prohibited. In contrast, when the Néel vector is along [100] and [110], the MSG is *Pnn'm'* and *Cmm'm'*, respectively. The MPG symmetry operations in *Pnn'm'* include $\boldsymbol{TC}_{2x}$, $\boldsymbol{C}_{2y}$ and $\boldsymbol{TC}_{2z}$, where $\boldsymbol{T}$ represents the time-reversal operation; i.e., $\boldsymbol{TC}_{2x}(\sigma_{yz}, \sigma_{zx}, \sigma_{xy}) = (-\sigma_{yz}, \sigma_{zx}, \sigma_{xy})$ and $\boldsymbol{TC}_{2z}(\sigma_{yz}, \sigma_{zx}, \sigma_{xy}) = (\sigma_{yz}, \sigma_{zx}, -\sigma_{xy})$. Thus, only σ_{zx} can be allowed. Given the fact that *Pnn'm'* and *Cmm'm'* consider different principal axes, one can conclude that the Hall vector is finite and directed along [010] (when the Néel vector || [100]) and [110] (when the Néel vector || [110]).

Supplementary Note 2, Curie-Weiss law fitting and calculation of effective moment:

According to the Curie-Weiss law, the magnetic order can be checked utilizing the relationship of magnetic susceptibility (χ) and absolute temperature (T) at the temperature regions above the magnetic ordering transitions, by:[29,30]

$$\chi = C / (T-\theta_W) \qquad (1)$$

where C is the Curie constant and θ_W is often referred to as the Weiss temperature (or Weiss constant). The fittings of Equation (1) with a positive, negative, and zero of θ_W indicate the ferromagnetic, antiferromagnetic, and paramagnetic phases, respectively. Furthermore, the constant C can be given by:

$$C = N_A \cdot \mu_0 \cdot \mu_{eff}^2 / (3k_B) \qquad (2)$$

where the $\mu_{eff}^2 = g_J \cdot (J+1) J \cdot \mu_B^2$, k_B is Boltzmann's constant, N_A the Avogadro constant, g_J the Landé g-factor, μ_B the Bohr magneton, J the angular momentum quantum number.

The Equation (2) calculated with the Gaussian units can give a: [29]

$$\mu_{eff} = (8C)^{1/2} \mu_B \quad [cgs] \qquad (3)$$

The $\chi^{-1} \sim T$ curves were fitted to obtain the C constants, and then the μ_{eff} were calculated.

Supplementary Note 3, Distinguish the side-jump and intrinsic anomalous Hall conductivity:

We try to distinguish the side-jump and intrinsic contributions of the σ_{xy}^M in the high conductivity region, which is generally considered through the following equation: [36-39]

$$\sigma_{xy}^{AHE} = -(\alpha \sigma_{xx0}^{-1} + \beta \sigma_{xx0}^{-2}) M \sigma_{xx}(T)^2 + b M \qquad (4)$$

Where, the M is the magnetization, $[\alpha \sigma_{xx0}^{-1} M \sigma_{xx}(T)^2]$, $[\beta \sigma_{xx0}^{-2} M \sigma_{xx}(T)^2]$, and $(b M)$ correspond to the anomalous anomalous Hall conductivity due to skew scattering, side-jump, and intrinsic mechanisms, respectively. The skew scattering in such a regime is negligible ($\alpha \approx 0$). We then carried out the fitting of $\sigma_{xy}^M \sim \sigma_{xx}(T)^2$ for the 10 nm, 20 nm, and 40 nm films respectively, as shown in Supplementary Fig. 9. Considering the M does not decrease too much with temperature increasing, the data of 3 K to 20 K were used. Note that the conductivity does not change too much within such a temperature region, and we can only obtain an estimation with the fitting by Equation (4), and an intrinsic anomalous Hall conductivity (σ_{xy}^{int}) of ~14 S/cm is obtained.

Supplementary Table 1, Spin order and moments of $Ru_{0.75}Cr_{0.25}O_2$ calculated with DFT with the b-axis doubled cell.

Cr at Ru-1 site			Cr at Ru-2 site	
Cr-1	1.8456 (μ_B)		Ru-1	0.1912 (μ_B)
Ru-2	-0.1911		Cr-2	-1.8456
Ru-1	0.0642		Ru-1	0.1912
Ru-2	-0.1911		Ru-2	-0.0642

Supplementary Table 2, Spin order and moments calculated with DFT for $Ru_{0.5}Cr_{0.5}O_2$.

Cr at Ru-1 site			Cr at Ru-2 site	
Cr-1	1.8434 (μ_B)		Ru-1	0.4031 (μ_B)
Ru-2	-0.4023		Cr-2	-1.8436

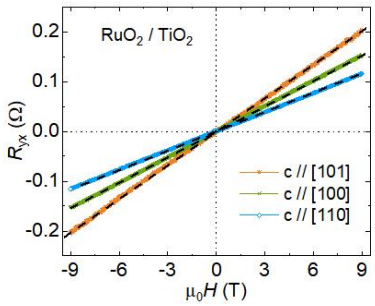

Supplementary Fig. 1, AHE in RuO_2 films grown on TiO_2. Magnetic field dependent Hall resistances (R_{yx}) of the RuO_2 films grown on TiO_2 with c axis along [100], [110], and [101] at 3 K.

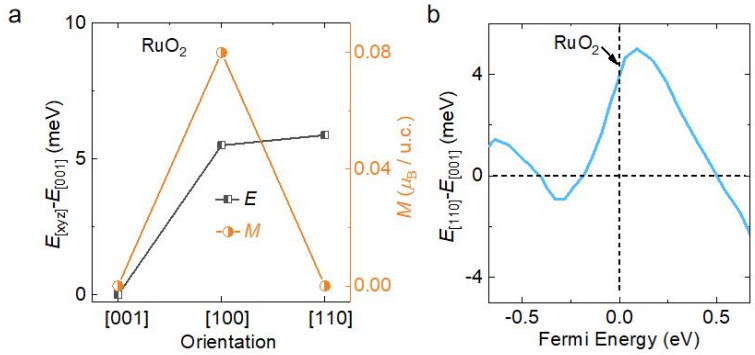

Supplementary Fig. 2, DFT+U calculations on the anisotropy of pure RuO_2. a, Calculated energy (E) and net moment (M) in pure RuO_2 with U = 3 eV depending on the initial orientation of the Néel vector. The state with Néel vector along [001] exhibits the lowest energy and no spontaneous moment. The states with Néel vector along [100] or [110] show about 5 meV higher energy, while the [100] case generates a spontaneous moment of 0.08 μ_B / unit cell. **b**, Calculated energy difference, $E_{[110]}$-$E_{[001]}$, in pure RuO_2 depending on the Fermi level. Data are obtained from reference 19.

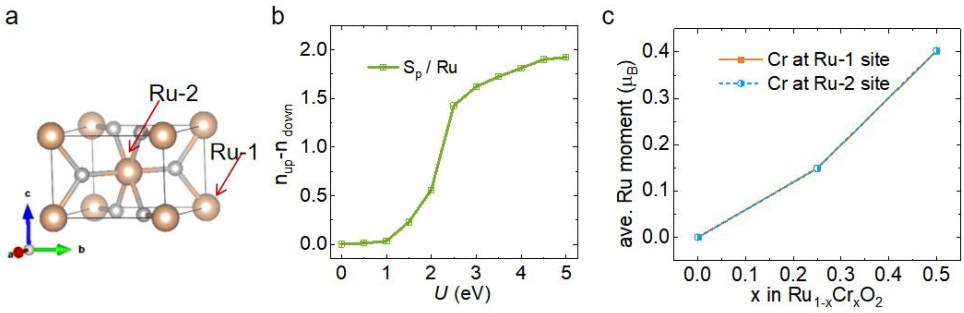

Supplementary Fig. 3, **Calculated results for $Ru_{1-x}Cr_xO_2$. a**, Crystal structure of one unit cell of RuO_2, where the two Ru sites are labeled as Ru-1 and Ru-2. **b**, DFT+DMFT result of the spin polarization (S_p=n_{up}-n_{down}) of RuO_2, plotted against the onsite Coulomb interaction U. For a small U (< 1 eV), S_p is almost negligible while it increases distinctly around U=2-3 eV. **c**, Average Ru moment with respect to the Cr doping level x in $Ru_{1-x}Cr_xO_2$, calculated with DFT.

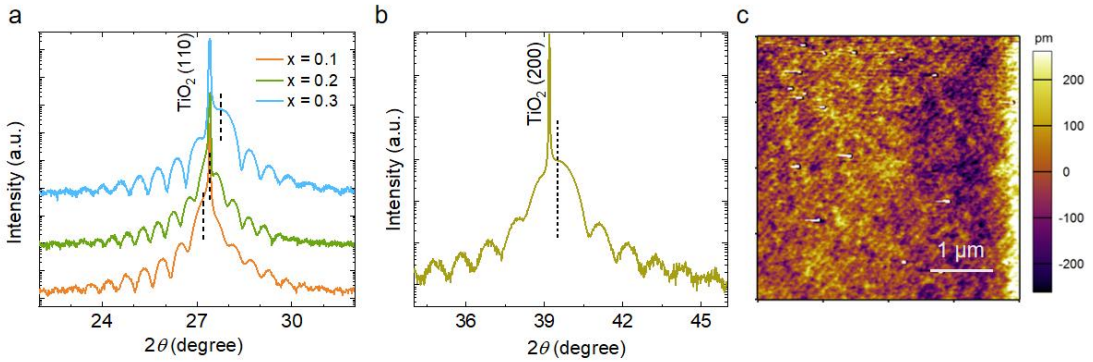

Supplementary Fig. 4, **Structure characteristics and surface morphology of the $Ru_{1-x}Cr_xO_2$ films**. **a**, XRD 2θ-ω curves of $Ru_{1-x}Cr_xO_2$ with x = 0.1, 0.2 and 0.3, measured around the TiO_2 (110). **b**, 2θ-ω curve of the $Ru_{0.8}Cr_{0.2}O_2$ film grown on TiO_2 (200). The diffraction peaks of the films are indicated by the d lines. **c**, surface morphology of the $Ru_{0.8}Cr_{0.2}O_2$ (110) film measured by atomic force microscopy (AFM).

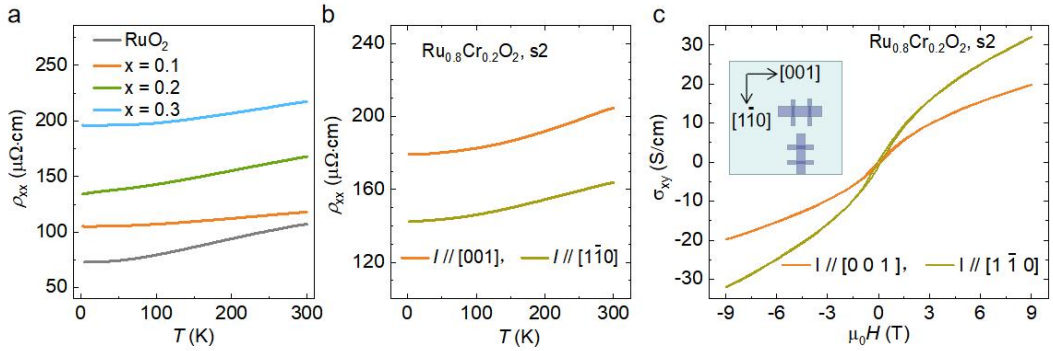

Supplementary Fig. 5, **Transport properties in $Ru_{1-x}Cr_xO_2$ (110) and the x = 0.2 film with current along different directions**. **a**, Temperature-dependent resistivities (*RT*) curves in $Ru_{1-x}Cr_xO_2$ films grown on TiO_2 (110). **b**, *RT* curves in $Ru_{0.8}Cr_{0.2}O_2$ measured with current along two orientations. **c**, σ_{xy} with magnetic field sweeping at 3 K in two current directions. The inset shows the configuration of the Hall measurements. S2, Sample No. 2 of the $Ru_{0.8}Cr_{0.2}O_2$ film.

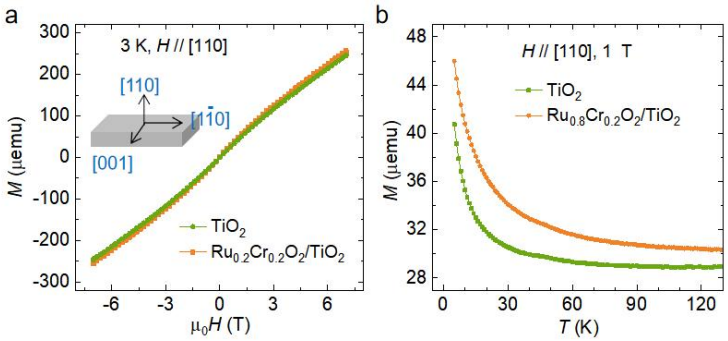

Supplementary Fig. 6, **Magnetization measurements in a $Ru_{0.8}Cr_{0.2}O_2$ (110) film.** **a**, **b**, Raw data for magnetization in the $Ru_{0.8}Cr_{0.2}O_2/TiO_2$ sample and a pure TiO_2 substrate with magnetic field (a) and temperature (b) dependence. The inset in (A) illustrates the crystal orientation of the film. The film thickness is 55 nm.

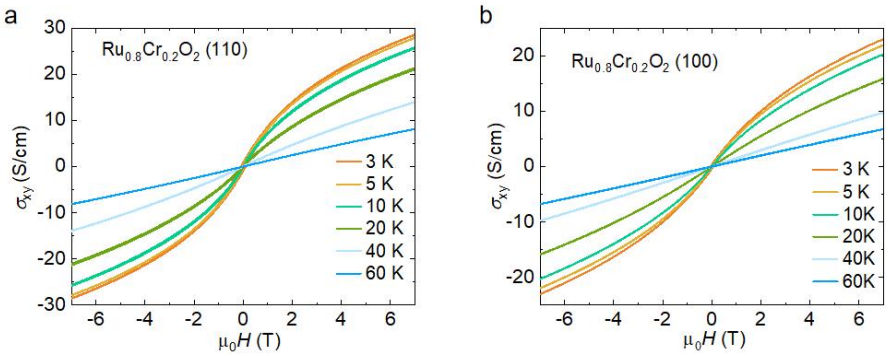

Supplementary Fig. 7, **Magnetic-field dependent Hall conductivity at various temperatures**. σ_{xy} with magnetic field dependence measured at a series of temperatures for $Ru_{0.8}Cr_{0.2}O_2$ films grown along the (110) and (100) orientations.

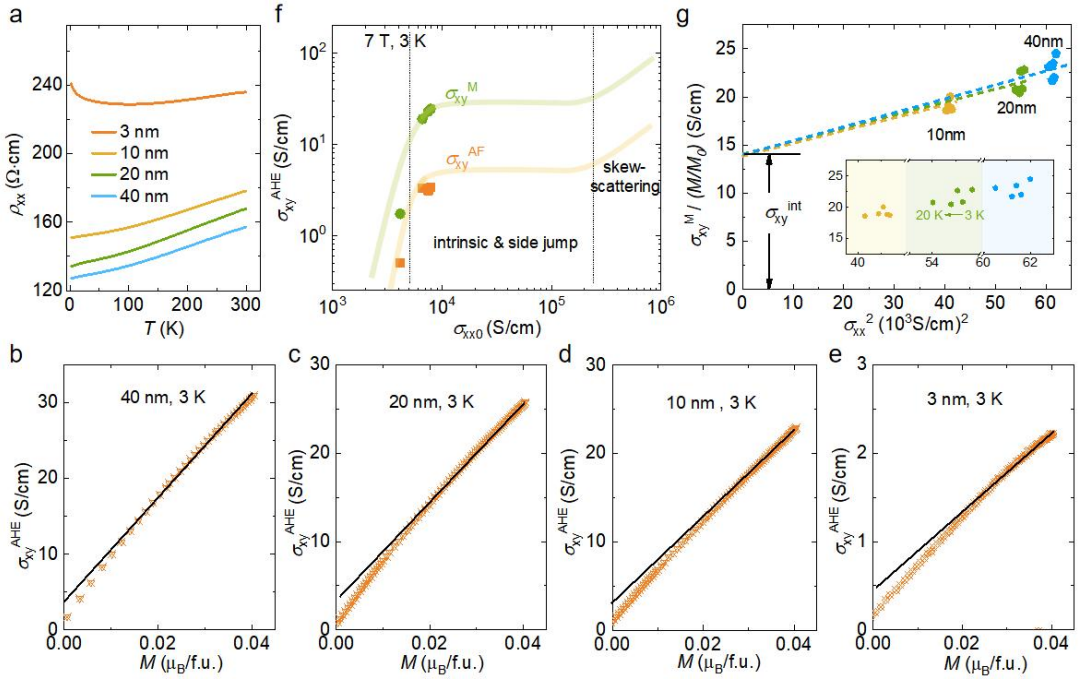

Supplementary Fig. 8, **Scaling of $\sigma_{xy}^{M} \sim \sigma_{xx}$ in the $Ru_{0.8}Cr_{0.2}O_2$ (110) films**. Evolution of anomalous Hall conductivity with the longitudinal conductivity from an itinerant metal to a localized state in $Ru_{0.8}Cr_{0.2}O_2$. **a**, *RT* curves of the $Ru_{0.8}Cr_{0.2}O_2$ films with thickness changing. **b-e**, Fittings of the σ_{xy}^{AHE} - *M* curves at high field regions to obtain the σ_{xy}^{M} and σ_{xy}^{AF} components for the films with a thickness of 40 nm (b), 20 nm (c), 10 nm (d), and 3 nm (e). **f**, Evolution of σ_{xy}^{M} and σ_{xy}^{AF} with the changing of σ_{xx0}. σ_{xx0} are set by the conductivity at 3 K. Dash lines denoting the boundaries of two regions, are given by reference 37. **g**, Linear fitting of the

normalized σ_{xy}^{M} - $\sigma_{xx}(T)^2$ with the data of 3 K - 20 K used for the 10 nm, 20 nm, and 40 nm films, respectively. The intercept denotes the intrinsic term of anomalous Hall conductivity. Inset, a zoom-in of the data.

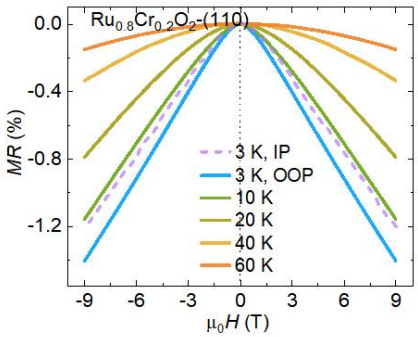

Supplementary Fig. 9, Magnetoresistivity (MR) measured for the $Ru_{0.8}Cr_{0.2}O_2$ (110) film. Out-of-plane (OOP) MR curves were measured at a series of temperatures and compared to the in-plane (IP) MR at 3 K. The IP field was along [001]. The current was along $[1\bar{1}0]$ for all measurements.